Journal of Power Sources 196 (2011) 4849–4858

Contents lists available at ScienceDirect

Journal of Power Sources

journal homepage: www.elsevier.com/locate/jpowsour

# Ion dynamics in the pseudocapacitive reaction of hydrous ruthenium oxide. Effect of the temperature pre-treatment

Suzana Sopčić[a], Zoran Mandić[a,*], György Inzelt[b], Marijana Kraljić Roković[a], Ernest Meštrović[c]

[a] Faculty of Chemical Engineering and Technology, Department of Electrochemistry, University of Zagreb, Maruličev trg 19, 10000 Zagreb, Croatia
[b] Department of Physical Chemistry, Eötvös Loránd University, Pázmány Péter sétány 1/A, 1117 Budapest, Hungary
[c] PLIVA Croatia Ltd., Research and Development, Prilaz baruna Filipovića 29, 10000 Zagreb, Croatia

ARTICLE INFO

*Article history:*
Received 24 September 2010
Received in revised form 2 December 2010
Accepted 17 January 2011
Available online 26 January 2011

*Keywords:*
$RuO_2$
Supercapacitors
EQCN
Temperature effect

ABSTRACT

Pseudocapacitive redox reaction of hydrous ruthenium oxide was investigated by the combined electrochemical and quartz crystal nanobalance measurements on gold support in $H_2SO_4$ and $Na_2SO_4$ solutions. The results show that the pseudocapacitance arises from at least two different Faradaic reactions with significant influence of double layer capacitance. All three processes simultaneously take place during charging/discharging reaction, but their contribution vary depending on the electrolyte used, the temperature pre-treatment and on the potential range. One Faradaic reaction releases protons during oxidation reaction resulting in the electrode mass decrease, while another Faradaic reaction results in the chemical binding of water leading to the mass gain during the oxidation reaction. The former reaction is favoured in acidic electrolyte and at lower anodic potentials, and the latter reaction proceeds predominantly in neutral media and at higher anodic potentials. The influence of annealing temperatures on the characteristics of the redox reaction of hydrous ruthenium oxide, as well as on its capacitance, was confirmed. It was demonstrated that specific capacitances of hydrous ruthenium oxide could achieve values as high as 1500 $F g^{-1}$, provided that conditions of good electronic conductivity among $RuO_2$ particles, as well as good electrical contact between gold and $RuO_2$, are met.



## 1. Introduction

Among various materials such as conducting polymers and transition-metal oxides, ruthenium oxide exhibits the most promising pseudocapacitive properties for the potential applications as an active electrode material in supercapacitors. It exhibits very reversible and reproducible electrochemical behaviour, the capability to store very high charge and to release it fast enough upon demand, as well as sufficient chemical and mechanical stability to undergo several thousands of charging/discharging cycles without significant deterioration of its charge storage ability and kinetics [1]. It is generally accepted that the electrochemical reaction accompanying the charging/discharging reaction of ruthenium oxide includes the simultaneous proton and electron exchange according to the equation:

$$RuO_x(OH)_y + ze^- + zH^+ \Leftrightarrow RuO_{x-z}(OH)_{y+z} \quad (1)$$

In the crystalline form ruthenium oxide is an electron-conductor with metallic-type conductivity [2] and due to relatively small interfacial area together with inaccessibility of bulk oxide redox sites, the specific capacitances obtained are relatively low [3,4]. On the other hand, much higher capacitances, up to 720 $F g^{-1}$, have been achieved with hydrous and amorphous form of ruthenium oxide [3]. Eq. (1) stipulates that both electronic conductivity and proton availability are necessary for good performance of ruthenium oxide in supercapacitor applications. Since the hydration of the ruthenium oxide promotes the proton conductivity, while at the same time hinders electron transport especially among the ruthenium oxide particles, it is obvious that the compromise between these two properties has to be made. It is now well established, and confirmed by several authors, that in order to achieve the maximal utilization of ruthenium oxide and extract as much charge as possible, two parameters, electronic and proton conductivity, should be optimized by annealing the amorphous $RuO_2 \cdot xH_2O$ at appropriate temperature [3,5–11]. Increased temperatures favour amorphous to crystalline phase transformation promoting the electronic conductivity, while at the same time removing physically bound water present in the material. Two opposing temperature effects result in optimal temperature of around 150 °C with maximal charge storage ability.

In order to further improve ruthenium oxide utilization and/or prevent unfavourable aggregation of ruthenium oxide particles several authors tried different $RuO_2$ preparation methods such as electrochemical deposition [8,12–14], oxidative chemical synthe-

* Corresponding author. Tel.: +385 1 4597164; fax: +385 1 3733640.
*E-mail address:* zmandic@fkit.hr (Z. Mandić).

0378-7753/$ – see front matter © 2011 Elsevier B.V. All rights reserved.
doi:10.1016/j.jpowsour.2011.01.070

sis [7], sol–gel process [3,15–19], electrostatic spray deposition [9,20], electrophoretic deposition [10], hydrothermal synthesis [21] and made various composite materials usually with different forms of carbon [5,15,16,22–29]. Hu et al. [5] recognized the importance of intra- and inter-particle electronic conductivity and prepared a composite material made of $RuO_2{\cdot}xH_2O$ and activated carbon. At low $RuO_2$ loadings they managed to achieve the specific capacitance as high as 1340 F $g^{-1}$. The importance of interparticle electronic conductivity was later confirmed by Kötz and co-workers [6] who used crystalline form of $RuO_2$ as a conductive matrix for amorphous $RuO_2$ particles. To the authors knowledge the highest specific capacitance ever reported for ruthenium oxide amounts to 1580 F $g^{-1}$ for activated carbon/hydrous $RuO_2$ composite on gold covered stainless steel electrode [27].

Another important property of $RuO_2$ electrode for the application in supercapacitors is its differential capacitance, i.e. the variation of specific capacitance with electrode potential. It has been observed in a number of papers that cyclic voltammograms of $RuO_2$ exhibit non-ideal capacitive response. In some cases, current reaches very low values especially at low anodic potentials with thermally untreated material [5–7,22]. Such behaviour indicates a more complex electrochemical behaviour of ruthenium oxide than shown by reaction 1. These observations were principally explained in the literature by two simultaneous reactions of different rates taking place during charging transformation of $RuO_2$ [30,31]. The fast process was associated with the charging of outer surface area, while the slow process was due to the charging of less accessible inner active sites. Sugimoto et al. [32] demonstrated that the overall pseudocapacitance of nano-crystalline $RuO_2$ could be deconvoluted even into three components, one non-Faradaic capacitive component (double layer capacitance) and two Faradaic components due to reversible and irreversible electrochemical reactions.

The investigations of the electrochemical reaction of $RuO_2$ by electrochemical quartz crystal nanobalance (EQCN) have been attempted in several papers [33–38]. In our previous work [33,34] we studied the redox processes of hydrated $RuO_2$ attached to the gold covered quartz electrode. Unlike the results obtained by Kim and Kim [35] and Atanasoski [36], who obtained monotonic mass loss during oxidation reaction with apparent molar masses of 3.2 and 56, respectively, our results showed that the various species participate in the reaction depending on the experimental conditions and that sometimes a mass gain and sometimes a mass loss accompanied the redox reaction. We observed that at least two different redox reactions are involved during charging/discharging reactions. A faster reaction corresponding to the reaction 1 leads to the mass release upon oxidation, and the other reaction is slow and proposed to proceed with the incorporation of oxygen into the hydrous $RuO_2$ matrix (Eq. (2)), thus leading to the mass gain upon oxidation. These results were in accordance with the results obtained by Vuković and Čukman [37] who found that electrodeposited ruthenium oxide exhibits a complex voltammetric reactions of non-stoichiometric origin which include various ruthenium oxyhydroxide species and water.

$$2RuO_2 + 2e^- + 2H^+ \Leftrightarrow Ru_2O_3 + H_2O \quad (2)$$

Recently, Kurzweil [39] proposed the dissociative water adsorption as the main reaction in the mechanism of the charging reaction of $RuO_2{\cdot}xH_2O$ by which during oxidation the protons are displaced from the OH sites and new oxide sites are formed.

In the present work we studied the properties and pseudocapacitive reaction of commercial $RuO_2{\cdot}xH_2O$ annealed at different temperatures up to 175 °C. Our intention was to reveal how the water content and crystallinity of the material influence the ion dynamics at the $RuO_2$/water interface and to give a further insight into the complexity of charging/discharging reaction of $RuO_2{\cdot}xH_2O$.

## 2. Experimental

Commercial hydrous ruthenium oxide, $RuO_2{\cdot}xH_2O$ (Aldrich) with average particle diameter of 10 nm is used as received or after annealing for 10 h at selected temperatures between 50 and 175 °C. All other chemicals were of p.a. quality. Solutions were prepared from bi-distilled water.

The crystal structure was confirmed by X-ray powder diffraction analysis. X-ray powder diffraction patterns were recorded using a PANanalytical X'PertPRO powder diffractometer at 40 mA, 40 kV, with monochromatized Cu Kα radiation. The diffraction peaks were detected with X'Celerator detector using the X'Pert software suite. The samples were scanned at the temperature of 20 °C with the diffraction angle $2\theta$ over the range of 3–70° with 0.008° steps, and 60 s per step.

Thermal analysis was performed using thermogravimetric analyzer TA instrument Q 500. The water content of the material at selected temperatures was estimated from the amount of weight loss at selected temperatures assuming that ruthenium oxide at 500 °C is completely anhydrous.

Simultaneous electrochemical and nanogravimetric measurements were carried out on 5 MHz AT-cut crystals of one inch diameter (Stanford Research Systems, SRS, USA) as working electrodes. Each side of the crystals was coated with titanium underlayer and gold. Only one side of the crystals with a projected surface area of $A = 1.22$ $cm^2$ was exposed to the electrolyte solution. The piezoelectrically active area was equal to 0.43 $cm^2$. The crystals were mounted in the holder made from Kynar and connected to a SRS QCM200 unit. The polished crystals were optically clear, according to the SRS certification their average surface roughness was ca. 5 nm. The Sauerbrey equation was used for estimation of the surface mass changes ($\Delta m$) from the frequency changes ($\Delta f$), with an integral sensitivity, $C_f = 5.66 \times 10^7$ Hz $cm^2$ $g^{-1}$. The experiments were carried out at room temperature ($T = 23 \pm 2$ °C).

The hydrous $RuO_2{\cdot}xH_2O$ particles annealed at selected temperatures were attached to the gold surface by wiping the electrode with a cotton swab containing the material [40], and then by making use of a drop of distilled water the particles were fixed. By the help of this procedure the crystals can be "glued" to the metal. This method of preparing the electrode produces a randomly distributed ensemble of particles on the gold, however, the distribution of particles was more or less uniform. Although the requirements (uniform and homogeneous surface layer) for the application of Sauerbrey equation are not perfectly met, on the basis of measured frequency values ($\Delta f$) a rough estimation can be done. The attached mass of $RuO_2{\cdot}xH_2O$ was determined by the change in the resonant frequency before and after the deposition of $RuO_2{\cdot}xH_2O$ and allowing it to dry prior to the measurement. Since the integral sensitivity of the EQCN was determined before the measurements, the possible error in the mass determination might come only from the uneven distribution of $RuO_2$ particles over the gold electrode which might be up to 10%. The attached masses of $RuO_2{\cdot}xH_2O$ particles for selected temperatures are given in Table 1.

For the calculation of the apparent molar mass ($M$) of the species released or incorporated in the material during redox reactions the following equation was used:

$$M = \frac{nFA\Delta f}{C_f Q} \quad (3)$$

where $n$ is the number of electrons transferred in the reaction, $F$ is Faraday constant, $A$ is the acoustically active surface area and $Q$ is the charge consumed. The value of charge obtained in the experiment was corrected taking into account the ratio of the piezoelectrically active surface area and the geometric surface area (the higher surface area that was exposed to the solution), and this value was used in Eq. (3) for the calculation of $M$.

**Table 1**
Masses, $m$, hydration number, $x$, and specific capacitances, $C_s$ ($\nu = 0.05\ V\ s^{-1}$), obtained in two electrolytes investigated ($H_2SO_4$ and $Na_2SO_4$).

| | $T$ (°C) | | | | | |
|---|---|---|---|---|---|---|
| | Room temp. | 50 | 75 | 100 | 130 | 175 |
| $m$ (μg) | 14.7 | 20.5 | 14.4 | 7.10 | 10.0 | 6.0 |
| $x$ | 1.6 | 1.3 | 1.1 | 0.9 | 0.6 | 0.4 |
| $C_s$ ($F\ g^{-1}$) ($H_2SO_4$) | 531 | 537 | 756 | 1102 | 1519 | 1259 |
| $C_s$ ($F\ g^{-1}$) ($Na_2SO_4$) | 269 | 204 | 259 | 313 | 346 | 350 |

Cyclic voltammetry experiments were carried out in a one-compartment cell by means of Potentiostat/Galvanostat PAR Model 263A. The reference electrode was saturated Ag/AgCl electrode and the counter electrode was a Pt-foil. All potential in this work are quoted against the Ag/AgCl reference electrode. For electrochemical impedance spectroscopy measurements lock-in amplifier PAR 5210 was connected to the above mentioned potentiostat. Measurements were performed in a wide frequency range from 0.01 Hz to 10 kHz and the amplitude of sinusoidal voltage was 5 mV. The impedance data were numerically processed with ZsimpWin3.10 software (Princeton Applied Research, USA) employing Down-hill simplex method for optimization.

## 3. Results and discussion

*Thermal analysis*. Fig. 1 shows TGA, differential thermal analysis (DTG) and mass change of ruthenium oxide sample upon fast heating to the selected temperatures. A continuous mass loss is observed during the whole temperature interval up to 500 °C. It is the confirmation of the hydrous nature of ruthenium oxide since thermal decomposition of ruthenium oxide to ruthenium metal takes place at much higher temperatures [41]. From the DTA results and according to the literature [24,42], two types of water could be distinguished in the hydrous ruthenium oxide. A weakly bound water is removed at temperatures below 100 °C (DTA peaks at 45 °C and 90 °C), while at higher temperatures the structural, chemically bound water is slowly lost. The water content of hydrous ruthenium oxide ($RuO_2{\cdot}xH_2O$) was estimated by mass loss at different temperatures and the results, in terms of hydration number, are given in Table 1. Maximal pseudocapacitance should be expected at water content of $x \sim 0.5$ [3,42–44] which is achieved in the present case when $RuO_2{\cdot}xH_2O$ is heated at about 150 °C.

*X-ray powder diffraction*. Simultaneously with the water removal at elevated temperatures, the transformation of amorphous to the crystalline form of ruthenium oxide takes place. Such behaviour has been observed by a number of investigators [3,24,43]. The crystallinity was determined by XRD and shown in Fig. 2 as a diffraction patterns of $RuO_2{\cdot}xH_2O$ at selected temperatures. At all investigated temperatures the material is amorphous in nature what is confirmed by the broad diffraction peaks. The identification of the samples by X-ray powder diffraction showed that the structures of $RuO_2$ correspond to the rutile structure with the space group $P4_2/mnm$ [45]. In the XRPD patterns the presence of peaks at 28.0° $2\theta$, 35° $2\theta$ and 54° $2\theta$, which belong to the diffraction from (1 1 0), (1 0 1) and (2 1 1) planes, respectively, is evident. The diffraction peaks of the thermally untreated sample are barely visible indicating more amorphous phase of $RuO_2{\cdot}xH_2O$, although previous PDF analysis showed that apparently amorphous $RuO_2{\cdot}xH_2O$ is, in fact, a composite of anhydrous rutile-like $RuO_2$ nanocrystals dispersed by boundaries of structural water associated with Ru–O bond [42]. Diffraction peaks become more and more pronounced as the heat-treatment temperature increases indicating the increase of the degree of crystallinity and the alteration of crystalline size. In addition, the intensity ratio between (1 1 0) and (1 0 1) peaks changes with the annealing temperature especially at the temperature of 175 °C. This tendency reflects systematic changes in unit $RuO_2$ lattice in three axial directions [45].

*Cyclic voltammetry*. Pseudocapacitive redox reaction of hydrous $RuO_2{\cdot}xH_2O$ annealed at different temperatures was further studied by electrogravimetry, i.e. simultaneous cyclic voltammetry and EQCN measurements. In our previous paper [34] we showed that the mechanism of the electrochemical reaction giving rise to high pseudocapacitance of hydrous $RuO_2{\cdot}xH_2O$ is more complex than one would conclude from a rather uniform rectangular shape of registered cyclic voltammograms. We confirmed the existence of different types of charge and also that charging/discharging reaction could not be described simply as simultaneous double proton–electron insertion/removal as described by Eq. (1). In order to help achieving the maximal utilization of hydrous $RuO_2{\cdot}xH_2O$ for its application in supercapacitor devices, it is necessary to gain deeper understanding of the mechanisms of the charging/discharging reaction of $RuO_2{\cdot}xH_2O$ and factors which govern its utilization especially when treated at different temperatures.

Fig. 3a–d display the cyclic voltammograms of the Au/$RuO_2$ electrodes annealed at selected temperatures in $H_2SO_4$ electrolyte together with the simultaneous quartz crystal resonant frequency change. Cyclic voltammograms show the usual electrochemical behaviour of hydrous $RuO_2{\cdot}xH_2O$. Relatively flat current profiles, as well as high currents in both anodic and cathodic directions, confirm the suitability of this material for the application in supercapacitors. Very broad anodic peak at about 0.5 V and its cathodic counterpart at around 0.35 V are commonly observed in the cyclic voltammograms of hydrous $RuO_2{\cdot}xH_2O$ [5–7,22] and it is generally accepted to be due to the reversible redox process accompanied by the sorption of protons and one or more water molecules [32,46]. Low currents at lower anodic potentials give rise to non-ideal capacitive behaviour and they are attributed to the physically bound water which forms the barrier for the electron transport among $RuO_2$ particles [5,6]. In contrast to the electrochemical responses of $RuO_2{\cdot}xH_2O$ in $H_2SO_4$ electrolyte, cyclic voltammograms taken in $Na_2SO_4$ electrolyte (Fig. 4a–d) are characterized by considerably lower overall currents and by the absence of broad current peaks. The effect of the annealing of the $RuO_2{\cdot}xH_2O$ at increased temperatures before the measurements is twofold. Firstly, increasing temperatures help to remove bound water and thus promote electronic conduction between the $RuO_2$ particles flattening the current profile in $H_2SO_4$ electrolyte. The transition from non-ideal to almost ideal rectangular shape for $RuO_2{\cdot}xH_2O$ with the annealing temperature in $H_2SO_4$ electrolyte is shown in Fig. 5a where, in order to give more clear representation of the effect, the specific current is normalized in respect of the instantaneous current registered at 0.55 V. In $Na_2SO_4$ electrolyte the annealing procedure affects the registered current at higher anodic potentials in greater extent than it is the case for lower anodic potentials (Fig. 5b). Likewise, the electrochemical process taking place at higher anodic potentials is more sensitive to the bound water hindering overall rate of the reaction than the process occurring predominantly at less anodic potentials. Such behaviour is the confirmation that the pseudocapacitance of $RuO_2{\cdot}xH_2O$ is caused by the overlapping of at least two reversible redox processes [32,34,39].

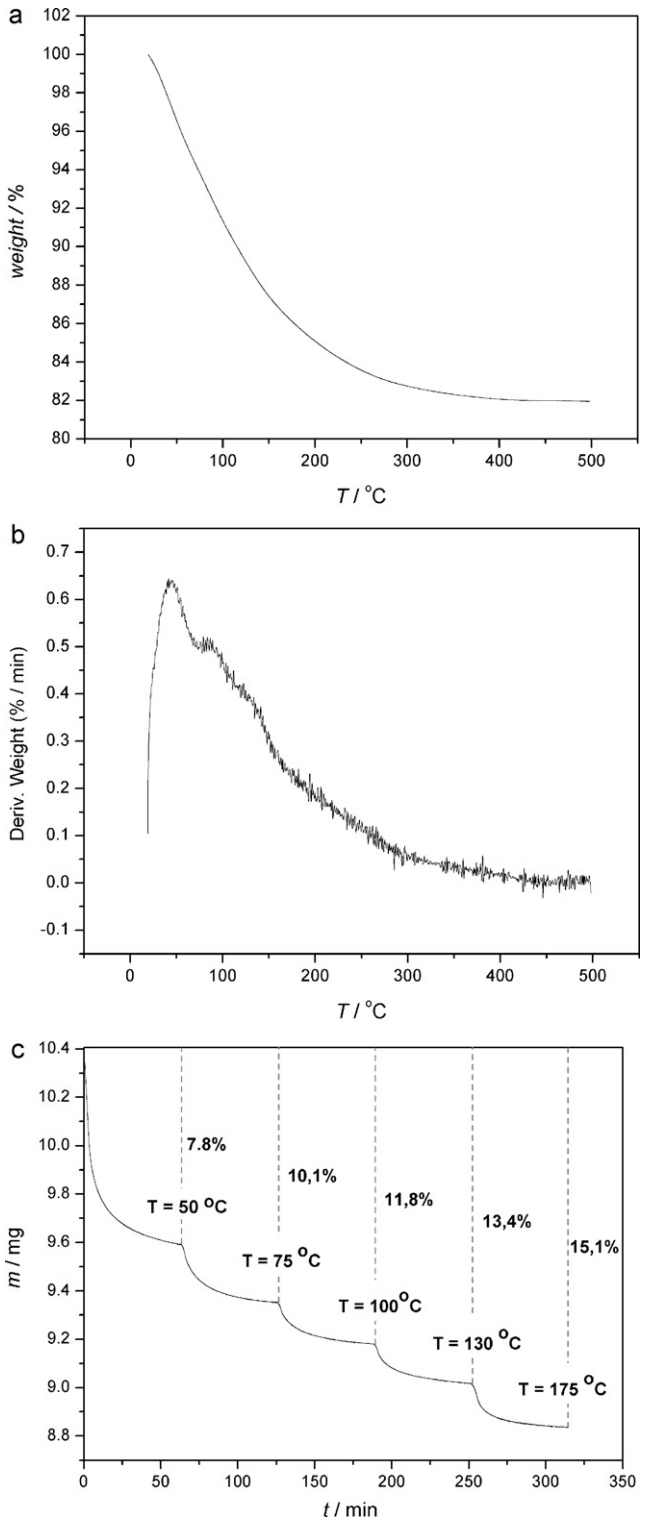


**Fig. 1.** Thermal analysis of hydrous $RuO_2$ used in this work. (a) Thermogravimetric analysis (TGA), (b) differential thermogravimetric curve and (c) mass change after fast heating to indicated temperatures. Temperature scan rate for (a) and (b) was 5 °C min$^{-1}$.

Another characteristic feature of the cyclic voltammograms shown in Fig. 3a–d, as well as in Fig. 4a–d, is the temperature effect on the capacitive current and consequently on the redox charge obtained. In both electrolytes the average current increases with the annealing temperature, very well known effect observed by many authors. The specific capacitances of $RuO_2{\cdot}xH_2O$ annealed at

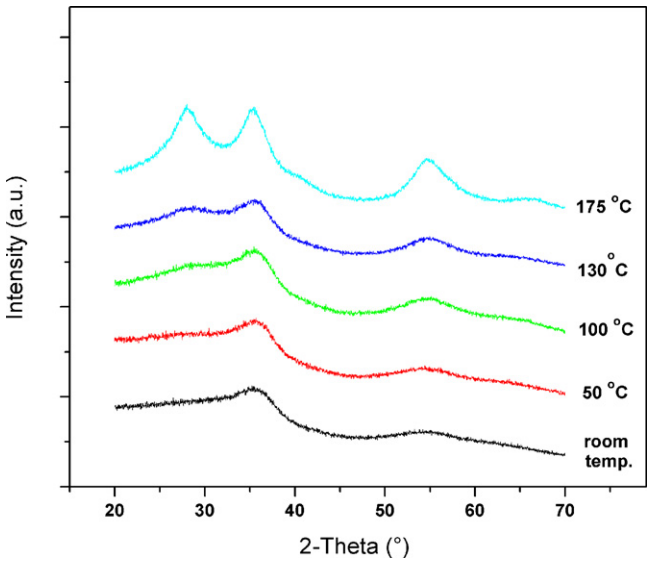


**Fig. 2.** XRD pattern of ruthenium oxide investigated in this work annealed at selected temperatures.

different temperatures were calculated from the cyclic voltammograms obtained in the potential range between 0.1 V and 1 V and at a scan rate, $\nu = 0.05\,V\,s^{-1}$ using the equation:

$$C_s = \frac{Q}{2\,\Delta E\,m} \tag{4}$$

where $Q$ is the sum of anodic and cathodic charges obtained by integration of the cyclic voltammograms in the potential interval $\Delta E$, and $m$ is the mass of the deposited $RuO_2{\cdot}xH_2O$. The amount of the deposited mass was calculated from the EQCN frequency change in dry state. The specific capacitance values obtained from cyclic voltammograms recorded at $0.05\,V\,s^{-1}$ for both $H_2SO_4$ and $Na_2SO_4$ electrolytes are given in Table 1. Specific capacitances in $H_2SO_4$ electrolyte increase with annealing temperature until temperature between 130 and 175 °C is reached. At 175 °C the specific capacitance drops. This is in a good agreement with already published results [3,6,11] which found the annealing temperature of 150 °C for preparing $RuO_2$ particles with optimal combination of crystallinity and water content to ensue a highest rate of proton and electron transport. Specific capacitances in $Na_2SO_4$ electrolyte also increase but their sensitivity to annealing temperature is not so high as in acidic medium. While with thermally untreated sample the specific capacitance in $Na_2SO_4$ electrolyte is half of that in acidic electrolyte, the specific capacitance for sample treated at 130 °C varies by factor of five. These results indicate that the optimization of proton and electron transport by controlling the crystallinity and water content of the sample influence the process under proton transport kinetics while the process taking place predominantly in neutral medium remains relatively unaffected.

The value of the specific capacitance of $1520\,F\,g^{-1}$ obtained for $RuO_2{\cdot}xH_2O$ in this work for the sample annealed at 130 °C is similar to the maximal capacitance of $1580\,F\,g^{-1}$ reported by Hu and Chen on gold covered stainless steel electrode [27]. Although it was found in some recent papers [28,29] that the primary particle size of cca 1 nm is a prerequisite for achieving the capacitances higher than $1000\,F\,g^{-1}$, our results show unusually high utilization of $RuO_2{\cdot}xH_2O$. It can be explained by the small masses deposited on the gold electrode and their uniform distribution ensuring intimate electrical contact between gold and each particle of $RuO_2{\cdot}xH_2O$ and overcoming the high interparticle electronic resistances that limit total charge. Namely, as proven in the literature [5,6] extremely high capacitances of $RuO_2{\cdot}xH_2O$ could be achieved if the mixture

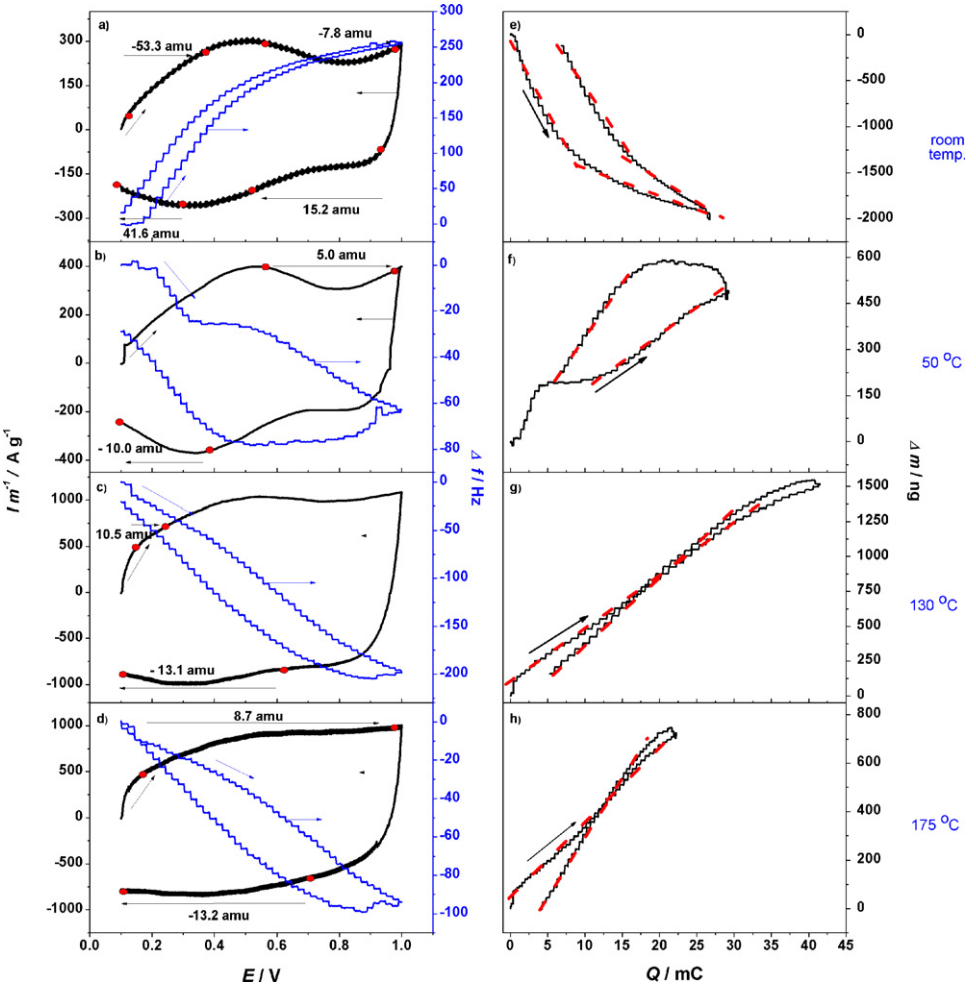


**Fig. 3.** (a)–(d) Cyclic voltammograms and quartz crystal resonant frequency change, (e)–(h) mass change vs. charge plots for Au/$RuO_2$ electrodes annealed at different temperatures indicated on graphs. Electrolyte: 0.5 M $H_2SO_4$, scan rate: 0.2 V $s^{-1}$.

of the small quantities of $RuO_2{\cdot}xH_2O$ with another material of sufficient electronic conductivity is prepared. In these cases, proton diffusion and electron conductivity were facilitated enough to achieve high utilization of the $RuO_2{\cdot}xH_2O$ in the mixture. In addition, it seems that gold support is important factor in achieving capacitances higher than 1500 F $g^{-1}$ since these were obtained only in our paper and in Ref. [27]. However, such high capacitances could not be explained by the electrochemical reactions given by Eqs. (1) and (2). It is very probable that, in addition to the Ru(III)/Ru(IV) redox transition, other valence states of ruthenium, most notably Ru(II) and Ru(V), might be involved in the overall process [5]. Also, double layer charging should not be neglected since it was already proven that its contribution to the overall charging process is significant.

*EQCN measurements*. Figs. 3a–d and 4a–d show simultaneous resonant quartz crystal frequency change recorded during the potential sweeps in $H_2SO_4$ and $Na_2SO_4$ electrolytes, respectively. While cyclic voltammetry provides an overall information of the charging behaviour of the investigated redox reaction, the EQCN results might reveal finer subtleties of the reaction mechanism. All samples, except thermally untreated $RuO_2{\cdot}xH_2O$, show resonant frequency decrease upon oxidation and frequency increase upon reduction reaction, meaning that the oxidation reaction is accompanied by the mass gain and the reduction reaction by the mass release. Similar trend is obtained in both electrolytes investigated. With the thermally untreated $RuO_2{\cdot}xH_2O$ opposite behaviour was observed in $H_2SO_4$ electrolyte (Fig. 3a), i.e. mass release during oxidation and mass gain during reduction reaction. Also, in the potential range investigated, at least two different dependencies of the frequency change vs. potential could be distinguished. When sample was treated at 50 °C the transitional behaviour between these two cases was observed (Fig. 3b). The frequency change due to the gold substrate is negligible concerning the overall EQCN response in the potential region of this study

From the EQCN results and cyclic voltammograms it is possible to construct the mass change vs. charge plots and from its slope to calculate the apparent molar masses of the exchanged species in different potential ranges. The corresponding $\Delta m$ vs. $Q$ curves obtained from the EQCN $\Delta f$ changes and displayed in Figs. 3a–d and 4a–d are given in Figs. 3e–h and 4e–h, respectively. With thermally untreated sample and with sample treated at 50 °C various slopes were obtained depending on the potential range and in some cases there is a gradual and continuous transition of the slope during anodic and cathodic cycles. All other samples show close to linear relationship between mass and charge. However, depending on the electrolyte used, temperature pre-treatment or hydration time, the curve levelling off at high anodic potentials, with practically no net mass release or gain, was observed. The effect is more pronounced in neutral $Na_2SO_4$ than in $H_2SO_4$ electrolyte although the hydration of the thermally treated samples of $RuO_2{\cdot}xH_2O$ results in the bending of $\Delta m$ vs. $Q$ curve giving in some cases even in the mass release at high anodic potentials (Fig. 6). For the thermally untreated sample and for sample treated at 50 °C two anodic (Ia and IIa) and two cathodic (Ic and IIc) potential

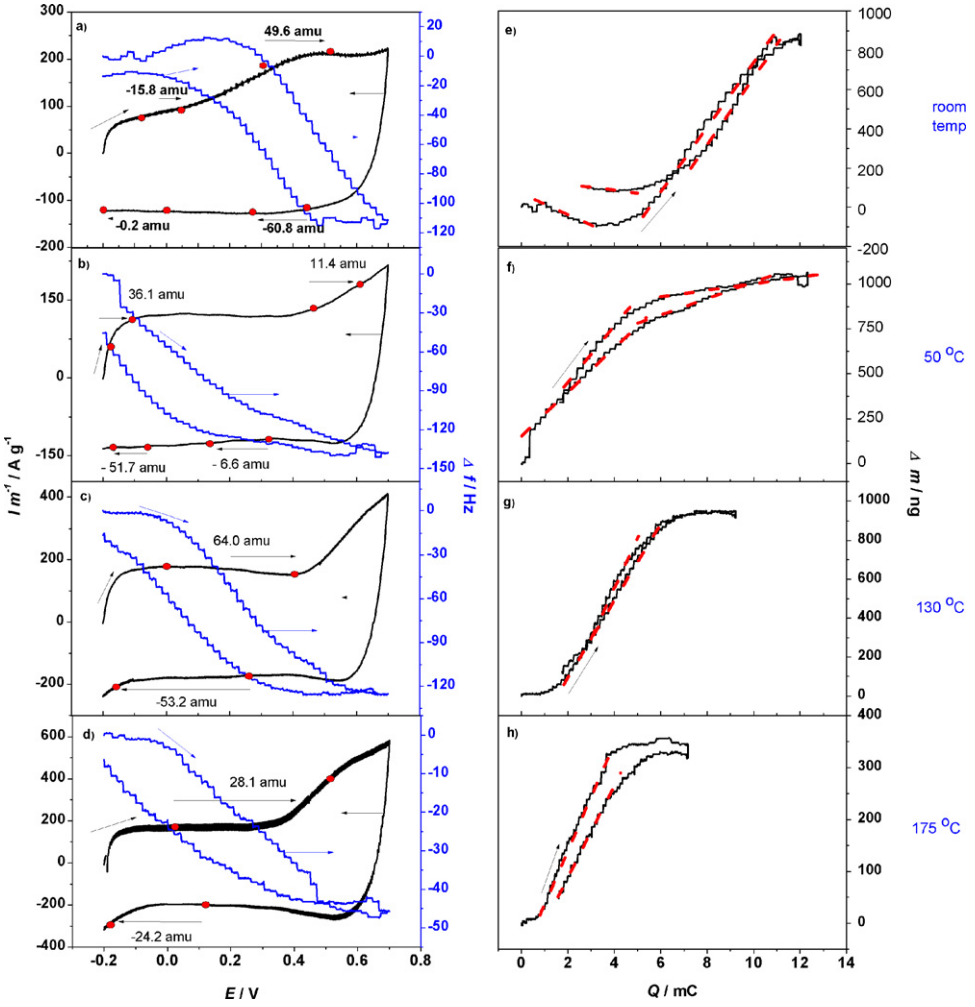


**Fig. 4.** (a)–(d) Cyclic voltammograms and quartz crystal resonant frequency change, (e)–(h) mass change vs. charge plots for Au/$RuO_2$ electrodes annealed at different temperatures indicated on graphs. Electrolyte: 0.5 M $Na_2SO_4$, scan rate: 0. 2 V $s^{-1}$.

regions where $\Delta m$ vs. $Q$ curve shows linear behaviour were identified (Fig. 3e and f). All other samples exhibit one linear region in $H_2SO_4$ electrolyte and in $Na_2SO_4$ electrolyte additional linear region at high anodic potentials with zero or close to zero slope exists. The potential ranges and the corresponding molar masses are indicated on the corresponding cyclic voltammograms on the left side of the Figs. 3 and 4, and also in Table 2 for all annealing temperatures.

The amu values clearly indicate that different ionic species participate in the redox process of hydrous ruthenium oxide what is in accordance with the results of Vuković and Čukman [37], who identified several types of non-stoichiometric surface reactions on electrodeposited ruthenium including various ruthenium oxyhydroxide species and water. In our previous paper [34] we observed that $RuO_2{\cdot}xH_2O$ is in some cases subject to both mass loss and mass gain in a single anodic sweep and identified simul-

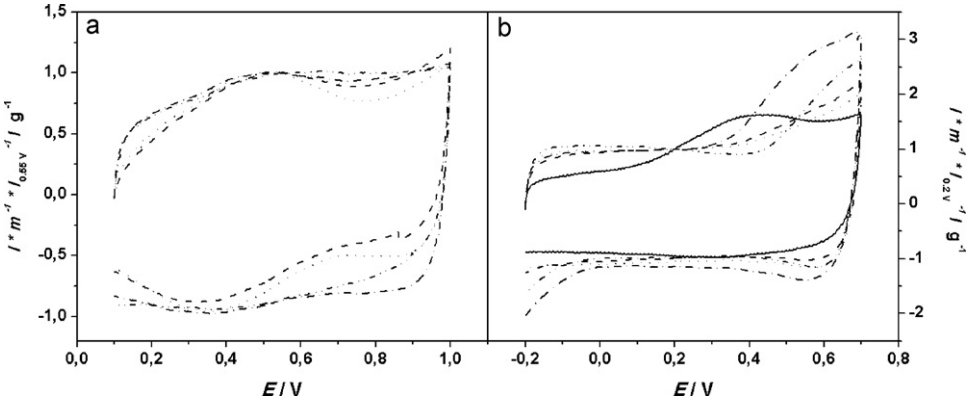


**Fig. 5.** Normalized cyclic voltammograms of $RuO_2{\cdot}xH_2O$ in (a) $H_2SO_4$ and (b) $Na_2SO_4$ supporting electrolytes at different pre-treatment temperatures. Room temperature (full line), 50 °C (dot), 100 °C (dash), 130 °C (dash-dot), 175 °C (dash-dot-dot). Scan rate: 0.1 V $s^{-1}$.

**Table 2**
Apparent molar masses, $M$ (amu), calculated from the corresponding anodic (Ia and IIa) and cathodic (Ic and IIc) potential ranges indicated in Figs. 3 and 4 for cyclic voltammograms obtained at scan rate, $\nu = 0.05\ V\ s^{-1}$.

| $T$ (°C) | 0.5 M $H_2SO_4$ | | 0.5 M $Na_2SO_4$ | |
|---|---|---|---|---|
| | Ia (Ic) | IIa (IIc) | Ia (Ic) | IIa (IIc) |
| Room temp. | −34.1 (32.9) | −7.8 (13.0) | −20.9 (−1.5) | 53.1 (−48.6) |
| 50 | 2.4 (−2.6) | – | 16.2 (−2.3) | 0 |
| 75 | 2.8 (−8.2) | – | 24.8 (−25.5) | 0 |
| 100 | 3.9 (−7.2) | – | 40.4 (−38.4) | 0 |
| 130 | 10.8 (−15.2) | – | 59.2 (−47.4) | 0 |
| 175 | 8.1 (−9.9) | – | 48.2 (−37.5) | 0 |

taneous occurrence of at least two types of charging reactions. These processes proceed at different rates and cannot be described simply as an adsorption of protons at surface and bulk material redox sites as proposed in several papers [30,31]. The results obtained in this work unambiguously confirm the existence of different types of pseudocapacitive reactions occuring simultaneously during charging/discharging reaction of hydrous $RuO_2{\cdot}xH_2O$. One reaction, leading to the mass release could be described by Eq. (1) and another which could be described by Eq. (2) results in the mass gain. The mass loss is expected upon oxidation if the reaction proceeding according to Eq. (1) is considered as a fast and dominant reaction giving rise to pseudocapacitance. According to the reaction mechanism given by Eq. (1), protons leave the hydrous oxide layer during oxidation dragging water which could come either from the hydrous layer or from the solution side. Up to four water molecules could be associated with proton in the proton hydration sphere and consequently the mass decrease between 1 and 73 amu per electronic charge could be expected depending on the origin of associated water molecules. The reaction mechanism given by Eq. (2) leads to the mass increase during oxidation and this reaction mechanism is recently termed a dissociative adsorption of water [39]. It results in a mass gain during oxidation reaction with the expected molar mass of the exchanged species of 8–9 amu per electronic charge. If these two reactions occur simultaneously, the apparent molar masses between these two values would be registered depending on the relative rates and contribution of these two reactions in the overall process. In addition to the scan rate dependence of apparent molar masses as shown previously [34], the contribution of these two processes depends also on other experimental variables such as electrolyte and pH, potential region and most notably on the temperature pre-treatment.

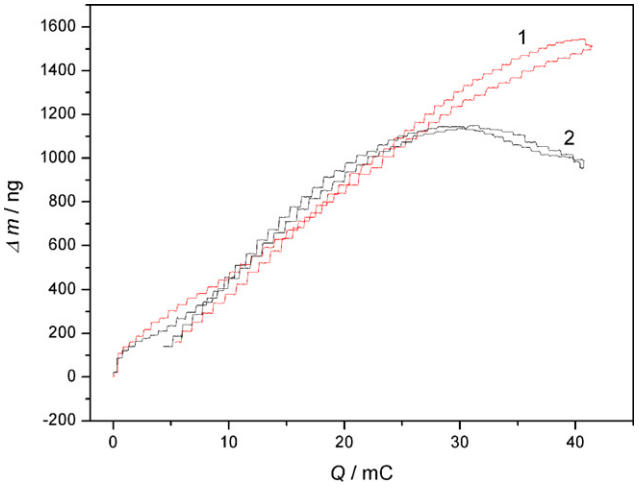


**Fig. 6.** Mass change vs. charge plots for Au/$RuO_2$ electrodes annealed at 130 °C before (1) and after (2) 24 h hydration in water.

The analysis of the results displayed in Figs. 3 and 4, as well as apparent molar masses shown in Table 2, reveals that thermally untreated $RuO_2{\cdot}xH_2O$ has two distinct potential regions of $\Delta m$ vs. $Q$ dependence. In acidic media throughout the potential window during anodic sweep mass loss is observed indicating that the dominant reaction of amorphous and hydrated $RuO_2{\cdot}xH_2O$ is reaction 1. However, at the potentials in the region of the broad anodic current peak the mechanism of the oxidation changes and amu values change from −34 to approx. −8 (results obtained for scan rate of $0.05\ V\ s^{-1}$, Table 2). In neutral $Na_2SO_4$ electrolyte in the second anodic potential range the mass gain was registered with the apparent molar mass value of 53.1 amu. At less anodic potentials in neutral electrolyte (region Ia) apparent molar mass is negative although this value seems to be very sensitive to the exact electrode pre-treatment as well as to the cation present [34]. It is worth noting that in neutral $K_2SO_4$ solutions mass gain is observed even in Ia region too. Thus, in contrast to acidic media, pseudocapacitve reaction of $RuO_2{\cdot}xH_2O$ in neutral media follows dissociative adsorption of water (Eq. (2)) as a predominant mechanism of reaction. It follows that when going from neutral to acidic pHs, the charge resulting from Eq. (1) contributes as an additional charge resulting in very high capacitances in $H_2SO_4$ electrolyte.

Obviously, two reactions representing pseudocapacitance of $RuO_2{\cdot}xH_2O$ in $H_2SO_4$ electrolyte take place simultaneously during the course of charging/discharging reaction. As seen from the Table 2, annealing temperatures change their relative rates and contribution to the overall charge. Although a small bending of $\Delta m$ vs. $Q$ curves at high anodic potentials and with samples annealed at temperatures higher than 50 °C could be noticed, the linear relationship with positive amu values exists throughout the potential window investigated. However, regardless of the apparently uniform reaction, two regions of charge dependence on potential still exist as seen in Fig. 6 where the relationship between mass and charge changes slope in IIa region after keeping the electrode 24 h in water. It is interesting to note that amu values increase from 2.4 for the sample annealed at 50 °C to 10.8 for the sample annealed at 130 °C and then drop, the same trend observed for specific capacitances (Table 1). These results indicate that the increase in crystallinity of $RuO_2{\cdot}xH_2O$ caused by the temperature pre-treatment as well as removing water from the material favours dissociative adsorption of water in the overall charge. The similar trend is observed for pseudocapacitive reaction in $Na_2SO_4$ electrolyte but in this case the apparent molar masses of the species incorporated in the electrode in Ia potential region are much higher and increase from 16.2 to 59.2 amu when annealing temperature increases from 50 to 130 °C, respectively. Although a small contribution of the reaction 1 in neutral $Na_2SO_4$ electrolyte might not be neglected, the pseudocapacitive reaction of $RuO_2{\cdot}xH_2O$ under these conditions follows almost exclusively mechanism given by Eq. (2). However, such a high amu values going up to 60 cannot be simply described by Eq. (2) since it predicts the mass gain of about 8 amu per electron removed. It seems that together with the water inclusion, as predicted by Eq. (2), this reaction enables

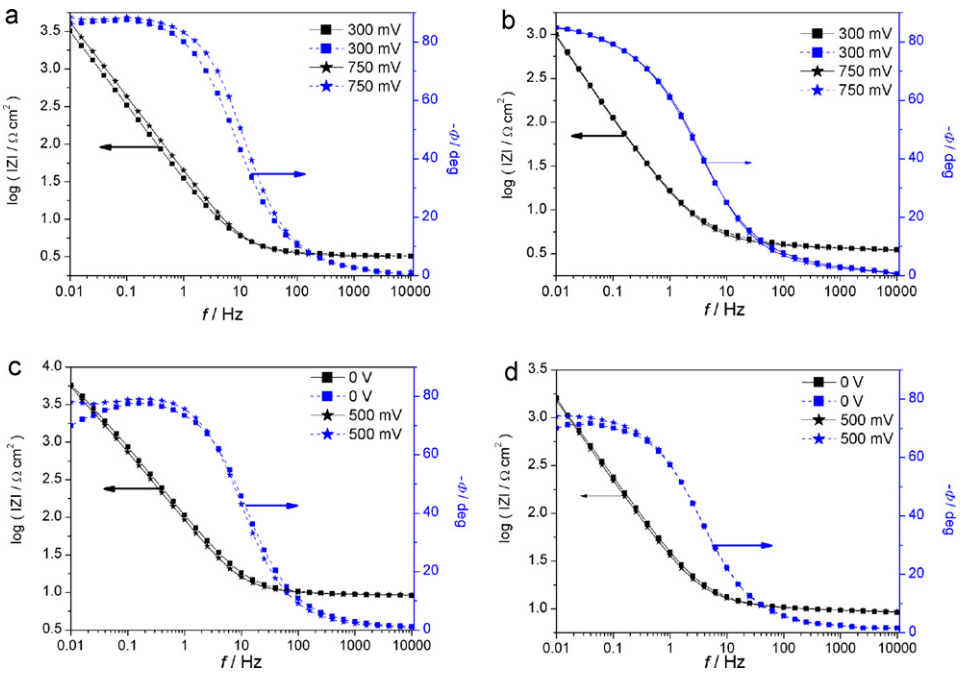


**Fig. 7.** Bode plots of impedance spectra of $RuO_2 \cdot xH_2O$ at two different potentials indicated on each plot: (a) room temperature and measured in $H_2SO_4$, (b) annealed at 175 °C and measured in $H_2SO_4$ electrolyte, (c) room temperature, $Na_2SO_4$ electrolyte, (d) annealed at 75 °C and measured in $Na_2SO_4$ electrolyte.

additional water molecules to be included as the physically bound water in the ruthenium oxide structure increasing its hydration. The hydration of the annealed samples was confirmed by the experiments in which the resonant frequency of $Au/RuO_2 \cdot xH_2O$ electrodes decreased and consequently its mass increased if it was kept in water for 24 h. The magnitude of the mass gain amounts up to 10% of the $RuO_2 \cdot xH_2O$ weight what corresponds approximately to the mass of the physically bound water removed at temperatures below the 100 °C (Fig. 1c). Since the contribution of Eq. (1) in the mechanism of the pseudocapacitve reaction in neutral electrolyte is negligible, the zero slope of $\Delta m$ vs. $Q$ curves obtained at higher potentials in the IIa potential region means that the charge in this potential region is dominated by the charging of double layer.

The EQCN results presented here are in accordance with the results of Sugimoto et al. [32] who managed to deconvolute the total charge of $RuO_2 \cdot xH_2O$ into the three components: electric double layer capacitance, a Faradaic component attributed to the irreversible redox reaction involving diffusion limited electroactive species and Faradaic component attributed to a reversible redox reaction involving electrosorption. The latter two Faradaic components could be described in this paper by Eqs. (1) and (2). Obviously, the reaction 1 is limited to the availability and to the rate of proton transport to the active ruthenium redox sites and it can proceed with sufficient rate in acidic media only and with samples with bound water which is able to facilitate the proton diffusion to the surface and into the grain boundaries or $RuO_2 \cdot xH_2O$ particles. This seems to be the determinal factor in achieving high charge of $RuO_2 \cdot xH_2O$ in acidic media. As soon as the water is removed the contribution of the reaction 1 relative to the rate of reaction 2 drops down and the amu values increase.

*Electrochemical impedance spectroscopy* (*EIS*). From the preceding sections it is clear that the nature of the species exchanged during pseudocapacitive reaction of $RuO_2 \cdot xH_2O$ depends not only on annealing temperature but also on the electrolyte and on potential range as well. Deeper insight into the reaction mechanism could be gained as well as some additional information could be extracted from the EIS measurements. We are particularly in checking how the temperature pre-treatment affects the capacitive properties of $RuO_2 \cdot xH_2O$.

Bode plots for investigated electrode (Fig. 7) exhibit typical shape of materials possessing supercapacitor properties. Resistive behaviour at high frequencies followed by almost pure capacitance at low frequencies could be conveniently described by equivalent circuit of the series combination of resistor and capacitor. Provided the series resistance is sufficiently low, such combination represents behaviour of ideal supercapacitor. However, there are several features in the different frequency regions of impedance spectra obtained in this work which deviate from ideality. At high frequencies a small semi-circle could be distinguished in some cases on $Z_{re}$ vs. $Z_{im}$ (Nyquist plot, not shown) impedance plots, especially with $RuO_2 \cdot xH_2O$ annealed at lower temperatures. The observed semi-circles were caused by the charge transfer resistance between Au and $RuO_2$ and/or among $RuO_2$ particles. Since charge transfer resistance could limit high-rate applications of supercapacitors, the influence of temperature pre-treatment on this parameter should not be neglected. In the intermediate and low frequency range, Warburg-type impedance terminated by capacitance could be identified. Such behaviour is frequently observed for materials possessing supercapacitor characteristics and originate either from redox reaction of a fixed amount of electroactive substance and/or finite diffusion of electroactive species. The best fit of our impedance data could be achieved using the model:

$$Z = R_{ohm} + \frac{R_{ct}}{C_{dl}} + Z_w \tag{5}$$

where $R_{ohm}$ is total ohmic resistance of the electrolyte and electrode, $R_{ct}$ – charge transfer resistance at gold/$RuO_2$ interface, $C_{dl}$ – double layer capacitance and $Z_w$ capacitively terminated diffusion line impedance [13,14,31,47]:

$$Z_w = C_w^{-1}\left(\frac{\tau_w}{j\omega}\right)^{1/2} \coth(j\omega\tau_w)^{1/2} \tag{6}$$

where $\tau_w$ is a time constant $\tau_w = R_w C_w$.

At low frequencies the observed phase shifts in the Bode phase-frequency diagram are less than the theoretical for ideal capacitor element, $\phi < -90^\circ$. Such non-ideality is manifested in $Z_{re}$ vs. $Z_{im}$ as a slope of the low-frequency domain less than 90° and is caused by the distribution of time constants, $\tau_w$, due to either heterogenity and non-uniformity of the surface and bulk redox active sites of $RuO_2{\cdot}xH_2O$ or different accessibility of protons to the deeper layers of $RuO_2{\cdot}xH_2O$.

Since EQCN results demonstrated the involvement of different kinds of charge taking place at different rates and at different regions of the potential window, the impedance measurements were carried out at two different potentials. The comparison of Bode plots for two different potentials, for two annealing temperatures and for both electrolytes investigated is shown in Fig. 7. Characteristic feature of the obtained results is that thermally untreated samples and samples treated at low temperatures show non-uniform capacitance magnitude with potential (Fig. 7a and c). Lower impedances and accordingly higher capacitances were obtained at 0.3 V and 0 V in $H_2SO_4$ and $Na_2SO_4$ electrolytes than at 0.75 and 0.5 V, respectively. With the increase of annealing temperatures this differences gradually diminish and the capacitance values become insensitive to potential. The difference between two impedance spectra almost completely disappears for the sample treated at 135 °C in $H_2SO_4$ electrolyte (Fig. 7b), while in $Na_2SO_4$ the superposition of the two spectra appears even at lower annealing temperatures, $T \geq 70$ °C (Fig. 7d). The variation of capacitance with potential is a consequence of the variation of the individual contribution of each of the three different charging mechanisms to the overall charge. Since the adsorbed and structural water content is a prerequisite for the facile diffusion of protons to the active redox sites, the treatment of $RuO_2{\cdot}xH_2O$ at increased temperatures slows down the rate of the reaction 1 resulting in a more uniform capacitance values with potential. Consequently, the reaction 1 has more dominant effect at lower anodic potentials. In neutral $Na_2SO_4$ electrolyte, reaction 1 is considerably diminished due to low availability of protons in the solutions and the capacitance is therefore more uniform with electrode potential with samples treated at lower temperatures before the measurement.

## 4. Conclusions

Despite its apparently monotonous cyclic voltammetry behaviour, the pseudocapacitive reaction of hydrous ruthenium oxide is a complex reaction consisting of two different Faradaic reactions superimposed on the double-layer capacitance. First Faradaic reaction, described as double proton–electron exchange reaction, is favoured in acid media and at lower anodic potentials. It proceeds with the mass release resulting in the EQCN resonant frequency increase during the anodic sweep. Another Faradaic reaction is described as a dissociative adsorption of water and proceeds with the incorporation of oxygen atom into the structure of ruthenium oxide leading to the mass gain and EQCN resonant frequency decrease. The latter reaction takes place predominantly in neutral media and at higher anodic potentials. The overall frequency changes depend on the relative contribution of these reactions in the total pseudocapacitance. The contribution is affected by the electrolyte used, temperature pre-treatment and potential window.

The importance of electronic resistance on the pseudocapacitive reaction is also demonstrated. It was confirmed that optimization of water content and inter-particle electronic resistance is achieved at temperatures around 150 °C. As a consequence of the optimization, the specific capacitances as high as 1500 F $g^{-1}$ are obtained with $Au/RuO_2$ electrode.

## Acknowledgments

This work is supported by bilateral program cooperation between Republic of Croatia and Hungary CRO-02/2006 as well as by national research projects No. 125-1252973-2576 from the Ministry of Science, Education and Sports of the Republic of Croatia as well as from the Hungarian National Office of Research and Technology (OMFB-00356/2007 and OM-00121-00123/2008), National Scientific Research Fund (OTKA K71771), and GVOP-3. 2.1-2004-040099. We appreciate very much a kind support from Prof. Zlata Hrnjak-Murgić and from the research projects No. 125-0821504-1976 and No. 125-1252971-3033 financed from the Ministry of Science, Education and Sports of the Republic of Croatia.

## References

[1] K.H. Chang, C.C. Hu, Appl. Phys. Lett. 88 (2006) 193102.
[2] L.F. Mattheiss, Phys. Rev. 13 (1976) 2433–2450.
[3] J.P. Zheng, P.J. Cygan, T.R. Jow, J. Electrochem. Soc. 142 (1995) 2699–2703.
[4] J.P. Zheng, T.R. Jow, J. Electrochem. Soc. 142 (1995) L6–L8.
[5] C.C. Hu, W.C. Chen, K.H. Chang, J. Electrochem. Soc. 151 (2004) A281–A290.
[6] O. Barbieri, M. Hahn, A. Foelske, R. Kötz, J. Electrochem. Soc. 153 (2006) A2049–A2054.
[7] K.H. Chang, C.C. Hu, J. Electrochem. Soc. 151 (2004) A958–A964.
[8] C.C. Hu, Y.H. Huang, K.H. Chang, J. Power. Sources 108 (2002) 117–127.
[9] I.H. Kim, K.B. Kim, J. Electrochem. Soc. 153 (2006) A383–A389.
[10] J.H. Jang, A. Kato, K. Machida, K. Naoi, J. Electrochem. Soc. 153 (2006) A321–A328.
[11] A. Foelske, O. Barbieri, M. Hahn, R. Kötz, Electrochem. Solid-State Lett. 9 (2006) A268–A272.
[12] C.C. Hu, Y.H. Huang, J. Electrochem. Soc. 146 (1999) 2465–2471.
[13] K. Kvastek, V. Horvat-Radošević, J. Electroanal. Chem. 511 (2001) 65–78.
[14] V. Horvat Radošević, K. Kvastek, M. Vuković, D. Čukman, J. Electroanal. Chem. 482 (2000) 188–201.
[15] J. Zhang, D. Jiang, B. Chen, J. Zhu, L. Jiang, H. Fang, J. Electrochem. Soc. 148 (2001) A1362–A1367.
[16] V. Panić, T. Vidaković, S. Gojković, A. Dekanski, S. Milonjić, B. Nikolić, Electrochim. Acta 48 (2003) 3805–3813.
[17] V. Panić, A. Dekanski, S. Gojković, V. Mišković-Stanković, B. Nikolić, Mater. Sci. Forum 453–454 (2004) 133–138.
[18] V. Panić, A. Dekanski, S. Milonjić, R. Atanasoski, B. Nikolić, Electrochim. Acta 46 (2000) 415–421.
[19] T.R. Jow, J.P. Zheng, J. Electrochem. Soc. 145 (1998) 49–52.
[20] I.H. Kim, K.B. Kim, Electrochem. Solid State Lett. 4 (2001) A62–A64.
[21] K.H. Chang, C.C. Hu, Electrochem. Solid-State Lett. 7 (2004) A466–A469.
[22] I.H. Kim, J.H. Kim, Y.H. Lee, K.B. Kim, J. Electrochem. Soc. 152 (2005) A2170–A2178.
[23] M. Min, K. Machida, J.H. Jang, K. Naoi, J. Electrochem. Soc. 153 (2006) A334–A338.
[24] M. Ramani, B. Haran, R. White, B. Popov, J. Electrochem. Soc. 148 (2001) A374–A380.
[25] V.V. Panić, A.B. Dekanski, R.M. Stevanović, J. Power Sources 195 (2010) 3969–3976.
[26] V. Panić, A. Dekanski, S. Gojković, S. Milonjić, V. Mišković-Stanković, B. Nikolić, Mater. Sci. Forum 494 (2005) 235–240.
[27] C.C. Hu, W.C. Chen, Electrochim. Acta 49 (2004) 3469–3477.
[28] V. Barranco, F. Pico, J. Ibanez, M.A. Lillo-Rodenas, A. Linares-Solano, M. Kimura, A. Oya, R.M. Rojas, J.M. Amarilla, J.M. Rojo, Electrochim. Acta 54 (2009) 7452–7457.
[29] F. Pico, J. Ibanez, M.A. Lillo-Rodenas, A. Linares-Solano, R.M. Rojas, J.M. Amarilla, J.M. Rojo, J. Power Sources 176 (2008) 417–425.
[30] S. Ardizzone, G. Fregonara, S. Trasatti, Electrochim. Acta 35 (1990) 263–267.
[31] J. Risphon, S. Gottesfeld, J. Electrochem. Soc. 131 (1984) 1960–1968.
[32] W. Sugimoto, T. Kizaki, K. Yokoshima, Y. Murakami, Y. Takasu, Electrochim. Acta 49 (2004) 313–320.
[33] S. Sopčić, M. Kraljić Roković, Z. Mandić, G. Inzelt, J. Solid State Electrochem. 14 (2010) 2021–2026.
[34] S. Sopčić, M. Kraljić Roković, Z. Mandić, A. Roka, G. Inzelt, Electrochim. Acta (2011), doi:10.1016/j.electacta.2010.10.035.
[35] I.H. Kim, K.B. Kim, J. Electrochem. Soc. 151 (2004) E7–E13.
[36] B.E. Conway, Electrochemical Supercapacitors, Kluwer Academic/Plenum Publishers, New York, 1999.
[37] M. Vuković, D. Čukman, J. Electroanal. Chem. 474 (1999) 167–173.
[38] M.C. Santos, L. Cogo, S.T. Tanimoto, M.L. Calegaro, L.O.S. Bulhoes, Appl. Surf. Sci. 253 (2006) 1817–1822.
[39] P. Kurzweil, J. Power Sources 190 (2009) 189–200.
[40] G. Inzelt, Z. Puskás, K. Németh, I. Varga, J. Solid State Electrochem. 9 (2005) 823–835.
[41] P.F. Campbell, M.H. Ortner, C.J. Anderson, Anal. Chem. 33 (1961) 58–61.
[42] W. Dmowski, T. Egami, K.E. Swider-Lyons, C.T. Love, D.R. Rolinson, J. Phys. Chem. B 106 (2002) 12677–12683.

[43] D.A. McKeown, P.L. Hagans, L.P.L. Carette, A.E. Russell, K.E. Swider, D.R. Rolison, J. Phys. Chem. B 103 (1999) 4825–4832.
[44] A. Mills, S. Giddings, I. Patel, C. Lawrence, J. Chem. Soc., Faraday Trans. 1 (83) (1987) 2331–2345.
[45] C.-E. Booman, Acta Chem. Scand. 24 (1970) 116–122.
[46] S. Trasatti, G. Buzzanca, J. Electroanal. Chem. 29 (1971) A1–A5.
[47] V. Horvat Radošević, K. Kvastek, M. Vuković, D. Marijan, J. Electroanal. Chem. 463 (1999) 29–44.